NANO LETTERS

Letter

Active Molecular Plasmonics: Controlling Plasmon Resonances with Molecular Switches

Yue Bing Zheng, Ying-Wei Yang, Lasse Jensen, Lei Fang, Bala Krishna Juluri, Amar H. Flood, Paul S. Weiss, J. Fraser Stoddart, and Tony Jun Huang

Nano Lett., **Article ASAP** • DOI: 10.1021/nl803539g

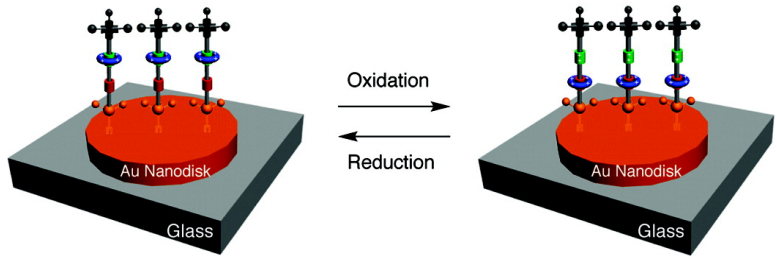

More About This Article

Additional resources and features associated with this article are available within the HTML version:

- Supporting Information
- Access to high resolution figures
- Links to articles and content related to this article
- Copyright permission to reproduce figures and/or text from this article

View the Full Text HTML

Nano Letters is published by the American Chemical Society. 1155 Sixteenth Street N.W., Washington, DC 20036

NANO LETTERS

XXXX
Vol. xx, No. x
-

Active Molecular Plasmonics: Controlling Plasmon Resonances with Molecular Switches

Yue Bing Zheng,[†] Ying-Wei Yang,[‡] Lasse Jensen,[§] Lei Fang,[||] Bala Krishna Juluri,[†] Amar H. Flood,[⊥] Paul S. Weiss,[§] J. Fraser Stoddart,*[,‡,||] and Tony Jun Huang*[,†]

Department of Engineering Science and Mechanics, The Pennsylvania State University, University Park, Pennsylvania 16802, California Nanosystems Institute and Department of Chemistry and Biochemistry, University of California, Los Angeles, California 90095, Departments of Chemistry and Physics, The Pennsylvania State University, University Park, Pennsylvania 16802, Department of Chemistry, Northwestern University, Evanston, Illinois 60208, and Department of Chemistry, Indiana University, Bloomington, Indiana 47405

Received November 21, 2008; Revised Manuscript Received December 10, 2008

ABSTRACT

A gold nanodisk array, coated with bistable, redox-controllable [2]rotaxane molecules, when exposed to chemical oxidants and reductants, undergoes switching of its plasmonic properties reversibly. By contrast, (i) bare gold nanodisks and (ii) disks coated with a redox-active, but mechanically inert, control compound do not display surface-plasmon-based switching. Along with calculations based on time-dependent density functional theory, these experimental observations suggest that the nanoscale movements within surface-bound "molecular machines" can be used as the active components in plasmonic devices.

Surface-plasmon-based nanophotonics,[1,2] or "plasmonics", can potentially guide and manipulate light at subwavelength scales and thereby allow the development of nanophotonic integrated circuits.[3−6] Although major breakthroughs have been made in plasmonic waveguides,[7−11] couplers,[12,13] and lenses,[14−16] a limited amount of research has been conducted on active plasmonic components, such as switches and modulators.[17−34] Recently, active plasmonic systems using metal nanoparticle/molecule complexes have been demonstrated and shown to have considerable promise as a new class of ultrasmall plasmonic components.[35−37] In these plasmonic systems, the molecules shift the localized surface plasmon resonances (LSPRs) of the metal nanostructures by changing the interactions between surface plasmon resonances and molecular resonances.[38−43] To date, the LSPR shifts in most of these systems are irreversible, one-way processes.[38−43] To realize the potential of molecular-level active plasmonics, a reversible shift of LSPRs needs to be demonstrated.[35] Herein, we take advantage of the reversible, controllable mechanical motions in molecular machines, such as switchable bistable rotaxanes, and demonstrate a molecular-level plasmonic switch that can be reversibly controlled by molecular machines.

When stimulated by light, electricity, or chemical reagents,[44] bistable rotaxanes[45−58] experience relative internal motions of their components, resembling superficially the operation of macroscopic machines.[44] The molecular formula and color-coded graphical representations of a disulfide-tethered bistable [2]rotaxane $\mathbf{2}^{4+}$ and its dumbbell precursor **1** are shown in Scheme 1. The bistable rotaxane $\mathbf{2}^{4+}$ is composed of a tetracationic cyclobis(paraquat-*p*-phenylene) ($CBPQT^{4+}$) ring, and a dumbbell-shaped component encompassing two recognition sites for the $CBPQT^{4+}$ ring—namely tetrathiafulvalene (TTF) and 1,5-dioxynaphthalene (DNP) units. The ground-state coconformation of $\mathbf{2}^{4+}$ has its TTF unit encircled by the positively charged $CBPQT^{4+}$ ring. Upon oxidation of the TTF unit, it becomes dicationic (TTF^{2+})

* To whom correspondence should be addressed: Professor J. Fraser Stoddart, Department of Chemistry, Northwestern University, 2145 Sheridan Rd, Evanston, IL 60208-3113; tel, (+1)-847-491-3793; fax, (+1)-847-491-1009; e-mail, stoddart@northwestern.edu. Professor Tony Jun Huang, Department of Engineering Science and Mechanics, Pennsylvania State University, University Park, PA 16802-6812; tel, (+1)-814-863-4209; fax, (+1)-814-865-9974; e-mail, junhuang@psu.edu.

† Department of Engineering Science and Mechanics, The Pennsylvania State University.

‡ California Nanosystems Institute and Department of Chemistry and Biochemistry, University of California.

§ Departments of Chemistry and Physics, The Pennsylvania State University.

|| Department of Chemistry, Northwestern University.

⊥ Department of Chemistry, Indiana University.

10.1021/nl803539g CCC: $40.75

Scheme 1. Molecular Formulas and Graphical Representations of Dumbbell **1** and Bistable [2]Rotaxane $\mathbf{2}^{4+}$[a]

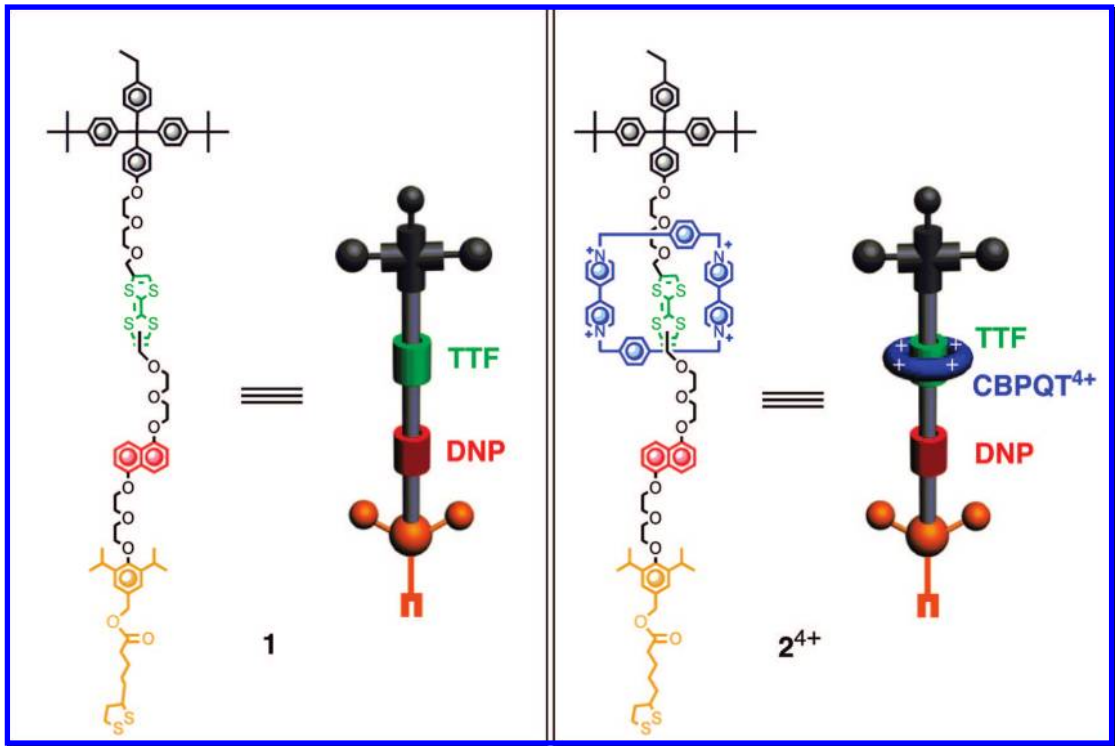

[a] The disulfide functional groups appended to **1** and $\mathbf{2}^{4+}$ were used to immobilize the molecules onto the Au nanodisk surfaces as chemically bound monolayers. Details on the synthesis of the bistable [2]rotaxanes and the dumbbells have been reported elsewhere.[58]

and repels the tetracationic ring electrostatically, thereby causing the ring's movement to the DNP unit. Subsequently, reduction of the TTF^{2+} dication back to its neutral (TTF) form causes the bistable rotaxane to return, from its metastable state coconformation to its initial starting state.

With prior knowledge of the controllable, reversible mechanical motions exercised precisely and cooperatively in nanoelectromechanical systems (NEMS)[50−56] and molecular electronics devices (MEDs)[57] at the molecular level by bistable rotaxanes, we anticipated their potential use in plasmonic switches. The electronic structure, and thus refractive index, of the bistable rotaxane are both strongly dependent on the underlying molecular structure. On the basis of the UV−vis−NIR extinction spectra (Figure 1a) of $\mathbf{2}^{4+}$ in its ground state and oxidized switched ($\mathbf{2}^{6+}$) states in *N*,*N*-dimethylformamide (DMF), we used the Kramers−Kronig relation[38] to determine the change in the refractive index (Δn) of the bistable rotaxane in the two states ($\mathbf{2}^{4+}$ and $\mathbf{2}^{6+}$)

$$\Delta n(\omega') = \frac{c}{\pi}\int_0^\infty \frac{\Delta\alpha(\omega)}{\omega^2 - (\omega')^2}\, d\omega \qquad (1)$$

where c is the speed of light, ω is the angular frequency ($\omega = 2\pi c/\lambda$, where λ is the wavelength of light), and $\Delta\alpha$ is the change in extinction coefficient between the two states of the bistable rotaxane (Figure 1a). Our calculations indicated a wavelength-dependent refractive index difference (Figure 1b) between the two states of $\mathbf{2}^{4+}/\mathbf{2}^{6+}$. Recently, it has been shown that the LSPR properties of metal nanoparticles

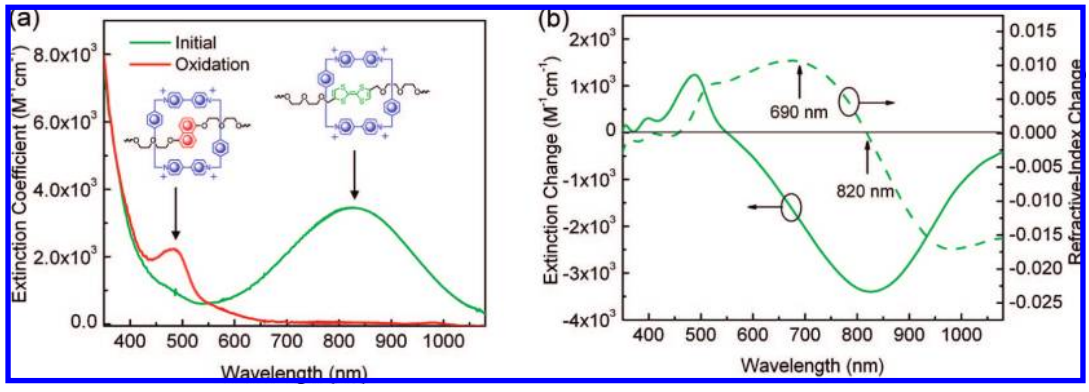

Figure 1. Extinction spectra and refractive-index change of $\mathbf{2}^{4+}$ in solution: (a) The extinction spectra of 2^{4+} in DMF (0.05 mM) before (green line) and after (red line) oxidation by 2 equiv of $Fe(ClO_4)_3$. (b) The oxidation-induced refractive-index change (dashed green line) of 2^{4+} was derived from the differential extinction spectrum (solid green line) by using the Kramers−Kronig relation.

change when resonant molecules are adsorbed to them.[38−40] The resulting LSPR shift is strongly dependent on the spectral overlap between the electronic resonance of the adsorbates and the plasmon resonance of the nanoparticles.[38] Consequently, one should be able to control actively the LSPR of the $\mathbf{2}^{4+}$-derivatized metal nanostructures by switching the position of the tetracationic ring and thus the electronic resonance of $\mathbf{2}^{4+}/\mathbf{2}^{6+}$. In line with this thinking, we have tuned the LSPR of Au nanodisks reversibly by controlling the redox states of the bistable rotaxane that were immobilized on the nanodisks' surfaces.

Ordered Au nanodisk arrays were fabricated on glass substrates using nanosphere lithography combined with reactive ion etching (see Supporting Information, Method S1 and Figure S1a). The nanodisks have a mean diameter of 140 ± 14 nm, a height of 20 ± 2 nm, and an array period of 320 ± 32 nm. The initial LSPR of the nanodisk arrays was controlled by varying the disks' diameters and heights. A monolayer of $\mathbf{2}^{4+}$ on the nanodisks was formed by incubating the nanodisks in a solution (0.1 mM in MeCN) of $\mathbf{2}\cdot 4PF_6$ for 2 days. The $CBPQT^{4+}$ ring encircles the TTF unit predominantly in the starting state of $\mathbf{2}^{4+}$ on the Au nanodisk surface (Figure 2a). Upon oxidation of the TTF unit, the electrostatic repulsion of the $CPBQT^{4+}$ ring and the stabilizing interactions afforded by the DNP unit provide a "push−pull" mechanism for the movement of the $CPBQT^{4+}$ ring within the dumbbell component of $\mathbf{2}^{6+}$. The switching behavior of $\mathbf{2}^{4+}$ in a monolayer on a Au surface has been demonstrated previously.[58]

The influence of $\mathbf{2}^{4+}/\mathbf{2}^{6+}$ on the plasmonic properties of Au nanodisks was investigated by monitoring the LSPR peak position with optical extinction spectroscopy. An HR4000 UV−vis−NIR spectrometer from Ocean Optics Inc. was used to record the extinction spectra of the nanodisks in air before and after the attachment of $\mathbf{2}^{4+}$ on the surfaces (see Supporting Information, Method S2 and Figure S2). After $\mathbf{2}^{4+}$ was self-assembled on the nanodisk surfaces by incubating the substrates in MeCN solution (0.1 mM $\mathbf{2}\cdot 4PF_6$) for 2 days, the LSPR peak wavelength red-shifted from 644.2 ± 0.2 to 690.4 ± 0.2 nm—this observation correlates with the increase in the surroundings' refractive index. The extinction spectra for the $\mathbf{2}^{4+}$-derivatized Au nanodisks in an oxidation/reduction cycle are shown in Figure 2b. The oxidant $Fe(ClO_4)_3$ in MeCN and reductant ascorbic acid in water have been successfully used in previous devices in which rotaxanes were self-assembled onto gold surfaces.[53] Oxidation of $\mathbf{2}^{4+}$ caused the LSPR peak to red shift from 690.4 ± 0.2 to 699.9 ± 0.2 nm, while reduction caused the peak to blue shift back to its initial position (Figure 2b). Slight deviations in the shapes of the spectra arose. These differences are believed to result from the switching of the bistable rotaxane molecules during the redox cycle. The reversible peak shift could be reproduced on repeated oxidation and reduction cycles.

The Kramers−Kronig analysis (Figure 1b) suggests that at 820 nm the refractive index change in $\mathbf{2}^{4+}$ before and after redox switching is close to zero. To test this hypothesis, we conducted similar experiments on $\mathbf{2}^{4+}$-derivatized Au nanodisks with an initial peak wavelength tuned to 818.9 ± 0.2 nm. Tuning of the initial peak to the specific wavelength of 818.9 ± 0.2 nm was realized by real-time chemical etching

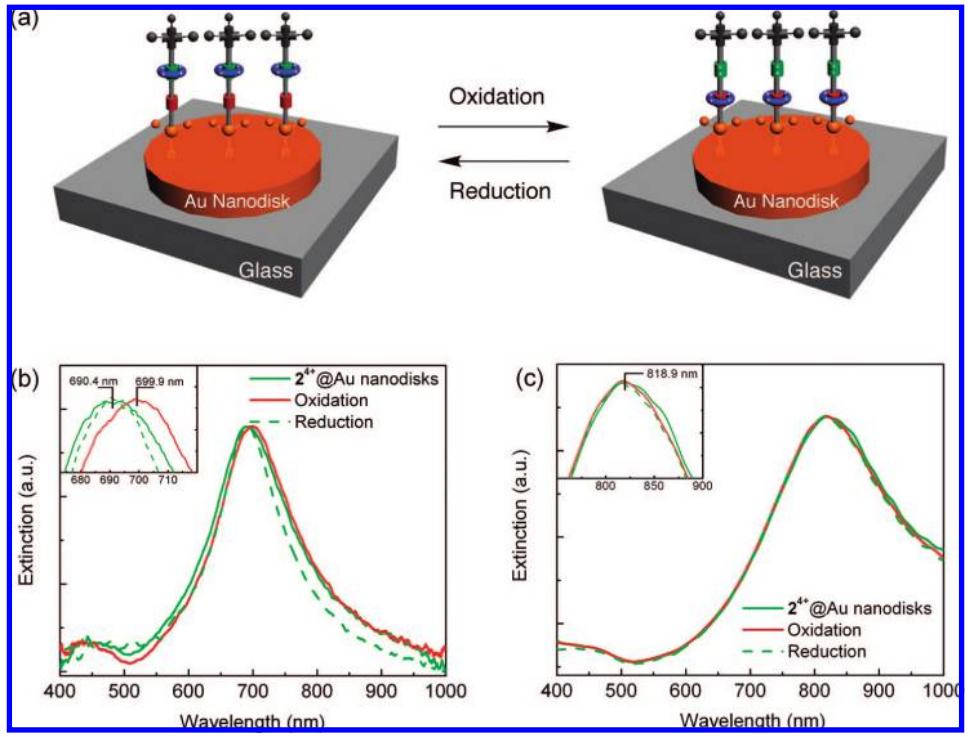

Figure 2. (a) Schematic of working principle of the molecular-machine-based active plasmonics. (b) Extinction spectra recorded from $\mathbf{2}^{4+}$-derivatized Au nanodisks in air with an initial peak wavelength of 690.4 ± 0.2 nm during the redox process. (c) Extinction spectra recorded from $\mathbf{2}^{4+}$-derivatized Au nanodisks with an initial peak wavelength of 818.9 ± 0.2 nm during the redox process. Insets in (b) and (c) are expanded views around the peak maxima in the spectra.

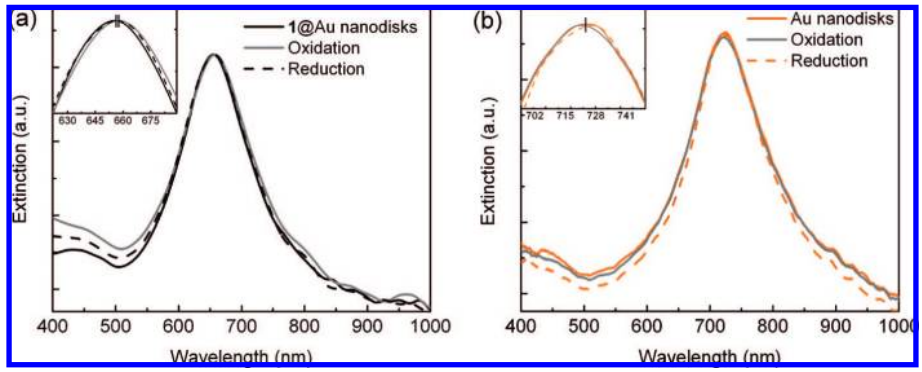

Figure 3. (a) Extinction spectra recorded from **1**-attached Au nanodisks in air during the redox process. A very small peak shift was observed during the redox process. (b) Extinction spectra recorded from bare Au nanodisks. No obvious peak shift was observed during the redox process. Insets in (a) and (b) are expanded views around the peak maxima in the spectra.

of the Au nanodisks. These nanodisks exhibited no shift of LSPR peak position during the redox cycle (Figure 2c). The redox-induced changes in peak positions in panels b and c of Figure 2 were consistent with the Kramers−Kronig analysis (Figure 1b), which reveals that the change of refractive index at a wavelength of 818.9 nm is close to zero, while a maximum increase in refractive index occurs around 690.4 nm.

In order to establish the unique correlation between the ring movement in $\mathbf{2}^{4+}$ and the shift in the LSPR peak position, two additional control experiments were carried out. In the first one, the redox-active but mechanically inert dumbbell **1**—instead of bistable rotaxane $\mathbf{2}^{4+}$—was adsorbed onto the Au nanodisks. The dumbbell **1** was self-assembled on the Au nanodisk surfaces by incubating nanodisks in CH_2Cl_2 solution (0.1 mM **1**) for 2 days. Upon oxidation, the **1**-attached nanodisks exhibited (Figure 3a) a LSPR peak shift of less than 2 nm, much smaller than the shift (Figure 2b) for $\mathbf{2}^{4+}$-derivatized nanodisks. In the second control experiment, bare Au nanodisks were employed and no peak shift was observed (Figure 3b) during the redox process. These results are consistent with the LSPR peak shift observed in $\mathbf{2}^{4+}$-derivatized Au nanodisk during the redox cycle correlating to the ring movement within the bistable rotaxane. They are also consistent with the switching mechanism proposed for similar bistable rotaxanes in other condensed phases associated with NEMS[50−56] and MEDs.[57]

Furthermore, we evaluated the refractive index of $\mathbf{2}^{4+}$ on Au nanodisks before and after oxidation ($\mathbf{2}^{6+}$). First of all, we calibrated the sensitivity of the LSPR to the changes in the surroundings' refractive index by recording the extinction spectra of the Au nanodisks when exposed to different environmental media of known refractive indices: air (n = 1), water (n = 1.33), acetone (n = 1.36), and optical oil (n = 1.63). The evolution of LSPR peak positions as a function of the surroundings' refractive index is shown in Figure 4 (indicated by empty circles), and linear fitting of the empty circles gives the sensitivity of the Au nanodisks as 145.9 nm/RIU (RIU: refractive index unit). On the basis of the calibrated sensitivity and the peak positions (Figure 2b) of $\mathbf{2}^{4+}$-derivatized Au nanodisks, the effective refractive index of $\mathbf{2}^{4+}$ around the wavelength of 690 nm was evaluated to be 1.31 ± 0.01 and 1.37 ± 0.01 before and after oxidation (Figure 4, indicated by triangles), respectively. The difference (0.06 ± 0.01) in the refractive index of bistable rotaxanes in the two states is larger than the value calculated using the Kramers−Kronig relation (Figure 1b). The discrepancy can be attributed to two factors. First, the measured extinction (Figure 1a) of $\mathbf{2}^{4+}$ was obtained in DMF solution, while the estimate of refractive index (Figure 4) was based on a monolayer of $\mathbf{2}^{4+}$ on the Au nanodisk surface recorded in air. Consequently, changes in solvation, counterions, orientation, and the coconformation of $\mathbf{2}^{4+}$, as well as the surface-plasmon-enhanced absorption in $\mathbf{2}^{4+}$,[35] would be expected. Second, the absorption spectra are available for only a limited wavelength range—from 200 to 1100 nm (see Figure 1a)—while an ideal calculation based on the Kramers−Kronig relation requires an integral with wavelengths from zero to infinity.[38]

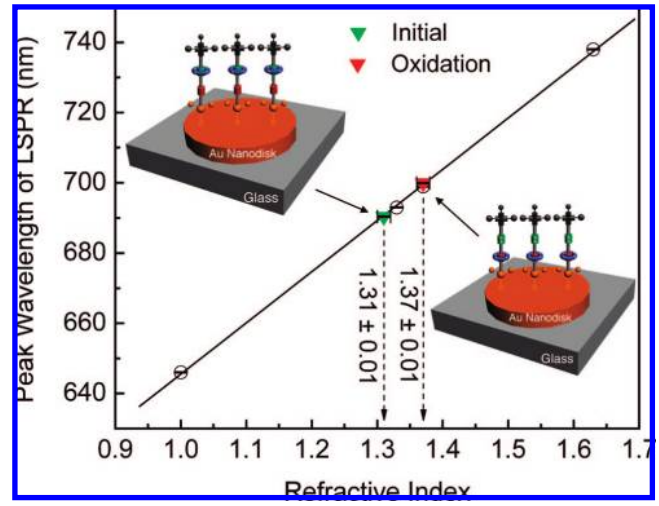

Figure 4. Experimental evaluation of the refractive index of the bistable [2]rotaxanes on Au nanodisks before and after oxidation. The empty circles are LSPR peak wavelengths for Au nanodisks exposed to environmental media with known refractive indices: air (n = 1), water (n = 1.33), acetone (n = 1.36), and optical oil (n = 1.63). The solid line is the fitted calibration curve, from which a sensitivity of 145.9 nm/RIU (RIU: refractive index unit) was obtained for the Au nanodisks. On the basis of the calibrated sensitivity and the LSPR peak wavelengths from Figure 2b, the effective refractive index of the bistable [2]rotaxanes in air was estimated to be 1.31 ± 0.01 and 1.37 ± 0.01 before and after oxidation, respectively.

To investigate the microscopic origin of the refractive index difference between the two states of the bistable rotaxane, we calculated the polarizability of $\mathbf{2}^{4+}$ using time-dependent density functional theory (TDDFT). We aimed to understand the difference in the polarizability between the two states (ground state and oxidized state) of the bistable [2]rotaxanes. In order to evaluate the polarizability at wavelengths near the electronic resonance—found experimentally at 820 nm—we used a recently developed method that includes a finite lifetime of the electronic excited states. The finite lifetime is expressed by a common damping parameter ($\Gamma = 0.1$ eV). The details of the method are described elsewhere.[59] All calculations presented in this work were carried out with a local version of the Amsterdam Density Functional (ADF) program package.[60] We used the Becke−Perdew (BP86) XC-potential and a triple-ζ polarized slater-type (TZP) basis set from the ADF library. In this set, the 1s core of N, O, C, and F and the 1s−2p core of P and S were kept frozen.

The size of the bistable [2]rotaxane $\mathbf{2}^{4+}$ used in the experiments was too large to perform a full-scale TDDFT calculation. In addition, the exact structure of $\mathbf{2}^{4+}$ when absorbed on the Au surface is unknown. To circumvent these difficulties and to provide a qualitative model for the frequency dependence of the polarizability ratio between the two states, we modeled the interactions of the $CBPQT^{4+}$ ring with two recognition sites. The ground-state molecule was simplified to the $CBPQT^{4+}$ ring at the TTF site ($CBPQT^{4+}$@TTF) plus the DNP unit. The oxidized state was modeled as the ring at the DNP site ($CBPQT^{4+}$@DNP) plus the TTF^{2+} dication. The four PF_6^- ligands were included in the calculations in order to neutralize the ring component.

An absorption band centered at 820 nm was identified (Figure 1a) when the ring was located at the TTF site, and it disappeared when $\mathbf{2}^{4+}$ was oxidized. The absorption band was caused by a charge-transfer (CT) excitation between the highest occupied molecular orbital (HOMO) of the TTF and the lowest unoccupied molecular orbital (LUMO) of the $CBPQT^{4+}$ ring (Figure 5a). Our TDDFT calculation is consistent with prior work,[61−63] and found the lowest transition of the $CBPQT^{4+}$@TTF complex to be at 0.75 eV with an oscillator strength of 0.094. This result corresponds to a transition from the HOMO of the TTF unit to the LUMO of the $CBPQT^{4+}$ ring, and the molecular orbitals are depicted in Figure 5a. Experimentally, this transition was found at 1.51 eV (820 nm), indicating that TDDFT underestimates the excitation energy by as much as 0.76 eV. It is well-known that TDDFT underestimates CT excitations in weakly interacting systems.[64] Therefore, we calculated the polarizability of the TTF−$CBPQT{\cdot}4PF_6$ at energies around 0.75 eV and then offset it by 0.76 eV to match the experimentally observed transition at 1.51 eV. Since there is only one transition in this region (600−1000 nm), we can fit the frequency dependence of the real part of the polarizability using a one-oscillator Lorentz model,[59] that is

$$\alpha_{CBPQT@TTF}(\omega) = \alpha^0 + \frac{b^2(\omega_0^2 - \omega^2)}{(\omega_0^2 - \omega^2)^2 + (2\Gamma)^2\omega^2} \qquad (2)$$

On the basis of the fitting results, we found $\alpha^0 = 788.83$ au and $b = 12.40$ eV. For the ground-state bistable rotaxanes, there is significant absorption (Figure 1a) in the region of 600−1000 nm. On the other hand, for the oxidized state, the CT band disappears and the absorption in the region is rather small. Therefore, we assume that the polarizability of the TTF−$CBPQT{\cdot}4PF_6$ complex is frequency dependent, and the rest of the system has a frequency-independent polarizability. On the basis of this assumption, the polarizability ratio of the two states of $\mathbf{2}^{4+}$ can be expressed as

$$\frac{\alpha^{ox}}{\alpha^{red}}(\omega) = \frac{\alpha_{CBPQT@DNP}(0) + \alpha_{TTF^{2+}}(0)}{\alpha_{CBPQT@TTF}(\omega) + \alpha_{DNP}(0)} \qquad (3)$$

Figure 5b is a plot of the calculated polarizability ratio as a function of wavelength. The polarizability ratio had a maximum value of 1.27, just blue of the CT transition at 772 nm. The minimum value of the polarizability ratio was found to be 0.72, red of the CT transition at 877 nm. The polarizability ratio close to the CT transition (820 nm) was 0.95. Using the Clausius−Mosotti equation[65] and the refractive index of $\mathbf{2}^{4+}$ based on the calibration curve in Figure 4, we established the polarizability ratio in terms of the refractive indices

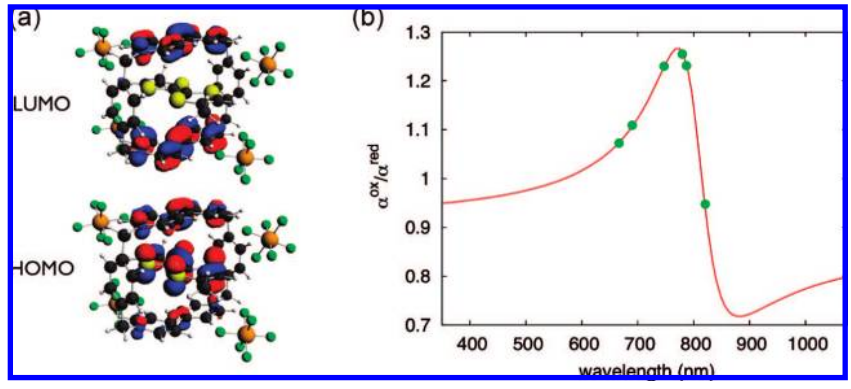

Figure 5. (a) The HOMO and LUMO for the TTF-$CBPQT{\cdot}4PF_6$ complex. The CT transition responsible for the absorption at 820 nm is a result of a transition from the HOMO on TTF to the LUMO on $CBPQT^{4+}$. (b) TDDFT-calculated polarizability ratio between the two states of $\mathbf{2}^{4+}$ as a function of wavelength. The solid line is a fit to the calculated values using a one-oscillator Lorentz model.

$$\alpha_{ox}/\alpha_{red} = [(n_{ox}^2 - 1)/(n_{ox}^2 + 2)][(n_{red}^2 + 2)/(n_{red}^2 - 1)] = 1.24 \quad (4)$$

The value of α_{ox}/α_{red} agreed well with the TDDFT-calculated maximum polarizability ratio (1.27). In addition, the calculated polarizability ratio (0.95) at the CT transition region (820 nm) was also in good agreement with the experimental results (Figure 2c) that showed no shift in the LSPR peak in the CT transition region. The excellent match between the two calculated results using two distinct methods—the TDDFT-based, *microscopic* model as compared with the refractive index-based, *macroscopic* model—was consistent with our hypothesis on the device's mechanism of operation.

Before bistable rotaxane-based active plasmonics can be used in practical applications, it is important to quantify the switching time of the molecules from one state to another. Thus far, the switching kinetics of bistable [2]rotaxanes have been studied in solution, in polymer matrices, and in self-assembled monolayers (SAMs).[58,66] Although it was shown[58] that the shuttling of $CBPQT^{4+}$ from TTF^{2+} to DNP was too fast to be measured experimentally, calculations using Constrained Molecular Dynamics Simulation revealed that the shuttling time was $\sim 10^{-7}$ s.[67] On the other hand, the shuttling of $CBPQT^{4+}$ from the DNP site back to the neutral TTF unit is much slower. Results from cyclic voltammetry measurements showed[58] that the lifetime of the metastable-state cocoformation of $\mathbf{2}^{4+}$ on a flat Au surface was 4.6 s at 293 K. More experimental and theoretical work will be needed to achieve better fundamental understanding of the molecular switching kinetics and to facilitate the design and synthesis of bistable rotaxanes with faster switching speeds and optimized optical properties.

In summary, we have demonstrated a molecular-level active plasmonic device that can be operated by switching the extinction properties of a bistable [2]rotaxane. The reversible switching in the LSPR properties of Au nanodisk arrays correlates with the chemically driven mechanical switching observed for surface-bound bistable [2]rotaxane molecules. This correlation was supported by control experiments and a TDDFT-based, microscopic model. The active molecular plasmonic system demonstrated here differentiates from the existing systems in the following aspects: (i) the active component, namely, bistable rotaxane, is one of a unique class of systems that can deliver controllable, reversible mechanical motions at the molecular level; (ii) the LSPR modulations observed here have been obtained for the first time with a monolayer (<10 nm thickness) of molecules, rather than from thin films or polymer matrices (>50 nm thickness);[28−31] and (iii) unlike some molecular plasmonic systems that only function in solution,[22,32−34] the bistable rotaxanes operate after being immobilized onto solid substrates.

Whenever a new application is demonstrated by bringing together two systems at the interface from the top-down and bottom-up, it is important to evaluate the scope of each element. In this context, the structures and properties of the wholly synthetic bistable rotaxanes can be customized and optimized. The flexibility in chemical structure enables the development of various bistable rotaxane-based molecular switches that have prescribed optical properties and can be switched by a range of external stimuli, i.e., chemical, electrochemical, or photochemical.[44] The latter two stimuli are particularly promising because (i) the act of switching is simple, (ii) the switching can take place without producing chemical waste, and (iii) electricity or light can be used to induce and to detect the molecular mechanical motions. We believe that the chemically driven redox process can be replaced with direct electrical or optical stimulation, a logical development that would establish a technological basis for the production of a new class of molecular-machine-based active plasmonic components for solid-state nanophotonic integrated circuits with the potential for low-energy and ultrasmall operations.

Acknowledgment. We thank Dr. Amanda J. Haes (The University of Iowa) for providing the MATHCAD code used in the Kramers−Kronig analysis and Dr. Vincent Crespi for helpful discussions. This research was supported by the Air Force Office of Scientific Research (AFOSR), the National Science Foundation (NSF), and the Penn State Center for Nanoscale Science (an NSF-funded MRSEC). Components of this work were conducted at the Pennsylvania State University node of the NSF-funded National Nanotechnology Infrastructure Network. One of the authors (Y.B.Z.) thanks the support of a KAUST Scholar Award and the Founder's Prize and Grant of the American Academy of Mechanics.

Supporting Information Available: Description of the methods. This material is available free of charge via the Internet at http://pubs.acs.org.

References

(1) Shalaev, V. M.; Kawata, S. *Nanophotonics with Surface Plasmons*; Elsevier BV: Oxford, 2007.
(2) Brongersma, M. L.; Kik, P. G. *Surface Plasmon Nanophotonics*; Springer: Berlin, 2007.
(3) Atwater, H. A.; Maier, S.; Polman, A.; Dionne, J. A.; Sweatlock, L. *MRS Bull.* **2005**, *30*, 385–389.
(4) Engheta, N. *Science* **2007**, *317*, 1698–1702.
(5) Ozbay, E. *Science* **2006**, *311*, 189–193.
(6) Zayats, A. V.; Smolyaninov, I. I.; Maradudin, A. A. *Phys. Rep.* **2005**, *408*, 131–314.
(7) Berini, P.; Charbonneau, R.; Lahoud, N. *Nano Lett.* **2007**, *7*, 1376–1380.
(8) Bozhevolnyi, S. I.; Volkov, V. S.; Devaux, E.; Laluet, J. Y.; Ebbesen, T. W. *Nature* **2006**, *440*, 508–511.
(9) Maier, S. A.; Andrews, S. R.; Martin-Moreno, L.; Garcia-Vidal, F. J. *Phys. Rev. Lett.* **2006**, *97*, 176805.
(10) Steinberger, B.; Hohenau, A.; Ditlbacher, H.; Stepanov, A. L.; Drezet, A.; Aussenegg, F. R.; Leitner, A.; Krenn, J. R. *Appl. Phys. Lett.* **2006**, *88*, 094104.
(11) Weeber, J. C.; Gonzalez, M. U.; Baudrion, A. L.; Dereux, A. *Appl. Phys. Lett.* **2005**, *87*, 221101.
(12) Lopez-Tejeira, F.; Rodrigo, S. G.; Martin-Moreno, L.; Garcia-Vidal, F. J.; Devaux, E.; Ebbesen, T. W.; Krenn, J. R.; Radko, I. P.; Bozhevolnyi, S. I.; Gonzalez, M. U.; Weeber, J. C.; Dereux, A. *Nat. Phys.* **2007**, *3*, 324–328.
(13) Knight, M. W.; Grady, N. K.; Bardhan, R.; Hao, F.; Nordlander, P.; Halas, N. J. *Nano Lett.* **2007**, *7*, 2346–2350.
(14) Dai, J. H.; Cajko, F.; Tsukerman, I.; Stockman, M. I. *Phys. Rev. B* **2008**, *77*, 115419.
(15) Fang, N.; Lee, H.; Sun, C.; Zhang, X. *Science* **2005**, *308*, 534–537.
(16) Smith, D. R.; Pendry, J. B.; Wiltshire, M. C. K. *Science* **2004**, *305*, 788–792.
(17) Andrew, P.; Barnes, W. L. *Science* **2004**, *306*, 1002–1005.
(18) Krasavin, A. V.; Zheludev, N. I. *Appl. Phys. Lett.* **2004**, *84*, 1416–1418.

(19) Chen, H. T.; Padilla, W. J.; Zide, J. M. O.; Gossard, A. C.; Taylor, A. J.; Averitt, R. D. *Nature* **2006**, *444*, 597–600.
(20) Pacifici, D.; Lezec, H. J.; Atwater, H. A. *Nat. Photonics* **2007**, *1*, 402–406.
(21) Pala, R. A.; Shimizu, K. T.; Melosh, N. A.; Brongersma, M. L. *Nano Lett.* **2008**, *8*, 1506–1510.
(22) Hall, W. P.; Anker, J. N.; Lin, Y.; Modica, J.; Mrksich, M.; Van Duyne, R. P. *J. Am. Chem. Soc.* **2008**, *130*, 5836–5837.
(23) Huang, W. Y.; Qian, W.; El-Sayed, M. A. *Nano Lett.* **2004**, *4*, 1741–1747.
(24) Chang, D. E.; Sorensen, A. S.; Demler, E. A.; Lukin, M. D. *Nat. Phys.* **2007**, *3*, 807–812.
(25) Suh, J. Y.; Donev, E. U.; Lopez, R.; Feldman, L. C.; Haglund, R. F. *Appl. Phys. Lett.* **2006**, *88*, 133115.
(26) Hendry, E.; Garcia-Vidal, F. J.; Martin-Moreno, L.; Gomez Rivas, J.; Bonn, M.; Hibbins, A. P.; Lockyear, M. J. *Phys. Rev. Lett.* **2008**, *100*, 123901.
(27) Wang, Z. C.; Chumanov, G. *Adv. Mater.* **2003**, *15*, 1285–1289.
(28) Hsiao, V. K. S.; Zheng, Y. B.; Juluri, B. K.; Huang, T. J. *Adv. Mater.* **2008**, *20*, 3528–3522.
(29) Leroux, Y.; Leroux, J. C.; Fave, C.; Trippe, G.; Felidj, N.; Aubard, J.; Hohenau, A.; Krenn, J. R. *ACS Nano* **2008**, *2*, 728–732.
(30) Kossyrev, P. A.; Yin, A.; Cloutier, S. G.; Cardimona, D. A.; Huang, D.; Alsing, P. M.; Xu, J. M. *Nano Lett.* **2005**, *5*, 1978–1981.
(31) Chapman, R.; Mulvaney, P. *Chem. Phys. Lett.* **2001**, *349*, 358–362.
(32) Sönnichsen, C.; Reinhard, B. M.; Liphardt, J.; Alivisatos, A. P. *Nat. Biotechnol.* **2005**, *23*, 741–745.
(33) Liu, G. L.; Yin, Y.; Kunchakarra, S.; Mukherjee, B.; Gerion, D.; Jett, S. D.; Bear, D. G.; Gray, J. W.; Alivisatos, A. P.; Lee, L. P.; Chen, F. F. *Nat. Nanotechnol.* **2006**, *1*, 47–52.
(34) Reinhard, B. M.; Sheikholeslami, S.; Mastroianni, A.; Alivisatos, A. P.; Liphardt, J. *Proc. Natl. Acad. Sci. U.S.A.* **2007**, *104*, 2667–2672.
(35) Dintinger, J.; Klein, S.; Ebbesen, T. W. *Adv. Mater.* **2006**, *18*, 1267–1270.
(36) Lee, J.; Hernandez, P.; Lee, J.; Govorov, A. O.; Kotov, N. A. *Nat. Mater.* **2007**, *6*, 291–295.
(37) Liu, G. L.; Long, Y. T.; Choi, Y.; Kang, T.; Lee, L. P. *Nat. Methods* **2007**, *4*, 1015–1017.
(38) Haes, A. J.; Zou, S. L.; Zhao, J.; Schatz, G. C.; Van Duyne, R. P. *J. Am. Chem. Soc.* **2006**, *128*, 10905–10914.
(39) Wurtz, G. A.; Evans, P. R.; Hendren, W.; Atkinson, R.; Dickson, W.; Pollard, R. J.; Zayats, A. V.; Harrison, W.; Bower, C. *Nano Lett.* **2007**, *7*, 1297–1303.
(40) Wiederrecht, G. P.; Wurtz, G. A.; Hranisavljevic, J. *Nano Lett.* **2004**, *4*, 2121–2125.
(41) Sugawara, Y.; Kelf, T. A.; Baumberg, J. J.; Abdelsalam, M. E.; Bartlett, P. N. *Phys. Rev. Lett.* **2006**, *97*, 266808.
(42) Fofang, N. J.; Park, T. H.; Neumann, O.; Mirin, N. A.; Nordlander, P.; Halas, N. J. *Nano Lett.* **2008**, *8*, 3481–3487.
(43) Ambjornsson, T.; Mukhopadhyay, G.; Apell, S. P.; Kall, M. *Phys. Rev. B* **2006**, *73*, 085412.
(44) Balzani, V.; Credi, A.; Ventur, M. *Molecular Devices and Machines*: Concepts and Perspectives for the NanoWorld; Wiley-VCH: Weinheim, 2008.
(45) Flood, A. H.; Ramirez, R. J. A.; Deng, W.-Q.; Muller, R. P.; Goddard, W. A., III; Stoddart, J. F. *Aust. J. Chem.* **2004**, *57*, 301–322.
(46) Aprahamian, I.; Yasuda, T.; Ikeda, T.; Saha, S.; Dichtel, W. R.; Isoda, K.; Kato, T.; Stoddart, J. F. *Angew. Chem., Int. Ed.* **2007**, *46*, 4675–4679.
(47) Aprahamian, I.; Dichtel, W. R.; Ikeda, T.; Heath, J. R.; Stoddart, J. F. *Org. Lett.* **2007**, *9*, 1287–1290.
(48) Jang, S. S.; Jang, Y. H.; Kim, Y.-H.; Goddard, W. A., III; Flood, A. H.; Laursen, B. W.; Tseng, H.-R.; Stoddart, J. F.; Jeppesen, J. O.; Choi, J. W.; Steuerman, D. W.; Delonno, E.; Heath, J. R. *J. Am. Chem. Soc.* **2005**, *127*, 1563–1575.
(49) Huang, T. J.; Tseng, H.-R.; Sha, L.; Lu, W.; Brough, B.; Flood, A. H.; Yu, B.-D.; Celestre, P. C.; Chang, J. P.; Stoddart, J. F.; Ho, C.-M. *Nano Lett.* **2004**, *4*, 2065–2071.
(50) Brough, B.; Northrop, B. H.; Schmidt, J. J.; Tseng, H.-R.; Houk, K. N.; Stoddart, J. F.; Ho, C.-M. *Proc. Natl. Acad. Sci. U.S.A.* **2006**, *103*, 8583–8588.
(51) Huang, T. J. *MRS Bull.* **2008**, *33*, 226–231.
(52) Huang, T. J.; et al. *IEEE Trans. Autom. Sci. Eng.* **2006**, *3*, 254–259.
(53) Liu, Y.; Flood, A. H.; Bonvallet, P. A.; Vignon, S. A.; Northrop, B. H.; Tseng, H.-R.; Jeppesen, J. O.; Huang, T. J.; Brough, B.; Baller, M.; Magonov, S.; Solares, S. D.; Goddard, W. A.; Ho, C.-M.; Stoddart, J. F. *J. Am. Chem. Soc.* **2005**, *127*, 9745–9759.
(54) Huang, T. J.; Brough, B.; Ho, C.-M.; Liu, Y.; Flood, A. H.; Bonvallet, P. A.; Tseng, H.-R.; Stoddart, J. F.; Baller, M.; Magonov, S. *Appl. Phys. Lett.* **2004**, *85*, 5391–5393.
(55) Nguyen, T. D.; Liu, Y.; Saha, S.; Leung, K. C.-F.; Stoddart, J. F.; Zink, J. I. *J. Am. Chem. Soc.* **2007**, *129*, 626–634.
(56) Patel, K.; Angelos, S.; Dichtel, W. R.; Coskun, A.; Yang, Y.-W.; Zink, J. I.; Stoddart, J. F. *J. Am. Chem. Soc.* **2008**, *130*, 2382–2383.
(57) Green, J. E.; Choi, J. W.; Boukai, A.; Bunimovich, Y.; Johnston-Halperin, E.; DeIonno, E.; Luo, Y.; Sheriff, B. A.; Xu, K.; Shin, Y. S.; Tseng, H.-R.; Stoddart, J. F.; Heath, J. R. *Nature* **2007**, *445*, 414–417.
(58) Tseng, H. R.; Wu, D. M.; Fang, N. X. L.; Zhang, X.; Stoddart, J. F. *ChemPhysChem* **2004**, *5*, 111–116.
(59) Jensen, L.; Autschbach, J.; Schatz, G. C. *J. Chem. Phys.* **2005**, *122*, 224115.
(60) Baerends, E. J.; et al. *Amsterdam Density Functional (ADF)*; http://www.scm.com, 2007.
(61) Jang, Y. H.; Hwang, S. G.; Kim, Y. H.; Jang, S. S.; Goddard, W. A. *J. Am. Chem. Soc.* **2004**, *126*, 12636–12645.
(62) Deng, W. Q.; Muller, R. P.; Goddard, W. A. *J. Am. Chem. Soc.* **2004**, *126*, 13562–13563.
(63) Deng, W. Q.; Flood, A. H.; Stoddart, J. F.; Goddard, W. A. *J. Am. Chem. Soc.* **2005**, *127*, 15994–15995.
(64) Drew, A.; Weisman, J. L.; Head-Gordon, M. *J. Chem. Phys.* **2003**, *119*, 2943–2946.
(65) Reitz, J. R.; Milford, F. J.; Christy, R. W. *Foundations of Electromagnetic Theory*; Addison-Wesley: Reading, MA, 1980.
(66) Choi, J. W.; Flood, A. H.; Steuerman, D. W.; Nygaard, S.; Braunschweig, A. B.; Moonen, N. N. P.; Laursen, B. W.; Luo, Y.; Delonno, E.; Peters, A. J.; Jeppesen, J. O.; Xu, K.; Stoddart, J. F.; Heath, J. R. *Chem. Eur. J.* **2006**, *12*, 261–279.
(67) Personal communication with Professor William A. Goddard at Caltech.

NL803539G